Electrical Property Heterogeneity at Transparent Conductive Oxide/Organic Semiconductor Interfaces: Mapping Contact Ohmicity Using Conducting-Tip Atomic Force Microscopy

Gordon A. MacDonald, P. Alexander Veneman, Diogenes Placencia, and Neal R. Armstrong*

Department of Chemistry and Biochemistry, University of Arizona, Tucson, Arizona 85721, United States

ABSTRACT We demonstrate mapping of electrical properties of heterojunctions of a molecular semiconductor (copper phthalocyanine, CuPc) and a transparent conducting oxide (indium–tin oxide, ITO), on 20–500 nm length scales, using a conductive-probe atomic force microscopy technique, scanning current spectroscopy (SCS). SCS maps are generated for CuPc/ITO heterojunctions as a function of ITO activation procedures and modification with variable chain length alkyl-phosphonic acids (PAs). We correlate differences in small length scale electrical properties with the performance of organic photovoltaic cells (OPVs) based on CuPc/C_{60} heterojunctions, built on these same ITO substrates. SCS maps the "ohmicity" of ITO/CuPc heterojunctions, creating arrays of spatially resolved current–voltage (J–V) curves. Each J–V curve is fit with modified Mott–Gurney expressions, mapping a fitted exponent (γ), where deviations from $\gamma = 2.0$ suggest nonohmic behavior. ITO/CuPc/C_{60}/BCP/Al OPVs built on nonactivated ITO show mainly nonohmic SCS maps and dark J–V curves with increased series resistance (R_S), lowered fill-factors (FF), and diminished device performance, especially near the open-circuit voltage. Nearly optimal behavior is seen for OPVs built on oxygen-plasma-treated ITO contacts, which showed SCS maps comparable to heterojunctions of CuPc on clean Au. For ITO electrodes modified with PAs there is a strong correlation between PA chain length and the degree of ohmicity and uniformity of electrical response in ITO/CuPc heterojunctions. ITO electrodes modified with 6–8 carbon alkyl-PAs show uniform and nearly ohmic SCS maps, coupled with acceptable CuPc/C_{60}OPV performance. ITO modified with C14 and C18 alkyl-PAs shows dramatic decreases in FF, increases in R_S, and greatly enhanced recombination losses.

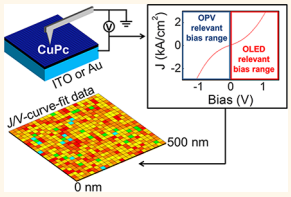

KEYWORDS: organic semiconductor · conducting-tip atomic force microscopy · ohmic contacts · organic solar cell · injection efficiency

Significant improvements in performance have recently been demonstrated for organic photovoltaic devices (OPVs) based on polymer and small-molecule active layers, as well as hybrid organic/inorganic active layers.[1–8] Device efficiency can significantly decrease in OPVs as device area increases, especially for electrodes where maintaining homogeneity in electrical properties is challenging, *e.g.*, in transparent conducting oxides (TCOs) such as indium–tin oxide and modified zinc oxides and for contacts based on assemblies of metallic nanowires or grids.[9–19] Device efficiency is also critically dependent on top and bottom electrode configuration and the injection efficiency (η_{inj}) of the contact electrodes, where η_{inj} is defined as the ratio of injected current over the theoretical maximum.[20–27] For nonohmic contacts, η_{inj} is always less than unity, leading to a decrease in current collection and a power loss for photovoltaic cells.[21] Using η_{inj} as a figure of merit for the "ohmicity" of electrical contact is complicated by two factors. First, one must empirically determine the theoretical maximum current for a given system. Second, η_{inj} is field dependent for injection-limited systems.[28] These limitations make using η_{inj} to compare different systems challenging. In this report we offer a more general approach for determination of the quality of electrical contact between electrodes and organic semiconductors (OSCs), on submicrometer to nanometer length scales, comparing those observations with the performance of simple planar heterojunction (PHJ) OPVs.

For both PHJ and bulk heterojunction (BHJ) device configurations the physical models developed thus far to explain OPV operation have often assumed that the contacts between both the top and bottom electrodes and the organic semiconducting materials exhibit high and uniform injection efficiency over large electrode areas and do not play a significant role in determining the current–voltage (J–V) response of these devices.[29–31] Recent studies, however, suggest that the electrical properties of the

* Address correspondence to nra@email.arizona.edu.

Received for review July 8, 2012 and accepted October 2, 2012.

Published online October 02, 2012
10.1021/nn303043y

most common transparent oxides used as hole-collection contacts, *i.e.*, indium–tin oxide, can be heterogeneous on 10–500 nm length scales.[12,13,16,17,19] While there are a number of reasons that ITO may not be the contact of choice in OPV platforms of the future, electrical heterogeneity in any contact will play a significant role in OPV device efficiency and in the ability to scale-up OPVs to practical energy conversion device areas, in a manner similar to effects seen for heterogeneous contacts in inorganic solar cells.[32,33] As such, the study of electrical heterogeneity in a contact like ITO is crucial for optimization of a variety of energy conversion and molecular electronic platforms.

Conductive-probe atomic force microscopy (C-AFM) techniques are well established for the characterization of the electrical properties of molecular electronic materials, and their contacts, on nanometer length scales.[19,27,34–38] In addition to the nanoscale resolution afforded by C-AFM using metallic tips as the top contact, the potential damage due to thermal deposition of a metallic top contact is avoided.[39,40] Standard C-AFM maps, however, show only the measured current at one tip–sample bias as a function of position along the surface plane. The measured current is a function of the total tip–contact–sample resistance and does not give information about the mechanism for charge transport through the electrode/OSC/C-AFM probe system. Additionally, these measurements are convoluted with topography of the contact, as the measured current is dependent upon the probe–sample contact area. The tip–sample contact can vary due to change in contact force, *i.e.*, as the probe moves over a topographic feature and the feedback mechanism must respond to restore the probe deflection, or as the probe moves over steep features and the sample contacts the sidewalls of the probe tip, rather than the apex of the probe tip, and from probe-to-probe variation in the tip radius of curvature.[41] In addition, the measured current will be affected by the local OSC thickness since the electric field (E) is determined by both the applied voltage and the distance between the top and bottom electrode. Thus variations in OSC thickness, due to crystallization for example, further obscure the underlining current transport mechanism, *i.e.*, whether or not a uniform ohmic contact has been made to the OSC.

Several investigators have recently demonstrated that spatially resolved J–V arrays can be used to map local variation in Schottky barrier height of ultrathin metal films and graphene layers on insulating substrates, in a technique termed scanning current spectroscopy (SCS).[42–45] SCS can be used as an imaging technique, analogous to force–volume and phase–volume imaging, where each pixel of the image is obtained by measuring a current–voltage curve and then fitting the J–V curve to an appropriate model and plotting the fitted parameter(s) as the image datum for that point.[46–49] For organic semiconductor thin films of device-relevant thicknesses, *i.e.*, films less than 100 nm in thickness, the J–V curves are expected to be dominated by space-charge-limited current at biases above a few millivolts if the electrode/semiconductor contact is ohmic.[21,35]

As reviewed by Malliaras and co-workers, an ohmic contact is defined as a contact in which the current is limited by charge transport through the organic semiconductor.[21] This implies that the rate at which charge can be injected (extracted) is not the rate-limiting step in charge transport through the system. Under these conditions, and assuming infinite planar electrodes and a non-field-dependent charge mobility, charge transport will be dictated by the Mott–Gurney (M–G) formalism, eq 1:

$$J = \frac{9}{8}\varepsilon\varepsilon_0\mu\frac{V^2}{L^3} \quad (1)$$

where J is the current density, V is the applied bias, $\varepsilon\varepsilon_o$ is the product of the dielectric constant and vacuum permittivity, μ is the charge carrier mobility, and L is the thickness of the organic semiconductor layer.[21]

Appropriate modifications to this relationship are required to account for the electrode geometries in C-AFM experiments; however the quadratic dependence of the current *versus* the voltage is retained.[35] Embedded in this relationship is the recognition that the mobility of the injected/harvested charge carrier is critical to determining whether, and at what applied fields, space-charge-limited currents will be achieved. The possible field dependence of charge mobility in the organic semiconductor can also make the distinction between ohmic and nonohmic behavior more complex.[50] When the electrical properties of the contact are not uniform and charge mobilities are low, the distribution of "active" *versus* "blocked" regions on the contact becomes critical in determining contact ohmicity. For an OPV under illumination this distribution of inactive sites on the contact can control the device series resistance and factors leading to reduced charge harvesting efficiencies, fill factor, and OPV efficiency.[16,51] It is also possible that contact heterogeneity can manifest as a distribution of trap states at the contact/organic interface, which can act like "blocked" regions if the trap is energetically deep enough. These sites may influence surface recombination rates and OPV efficiency in a fashion that may be seen as analogous to the effect of blocked sites on the electrode surface.[7,20,52–54]

We present here a conducting-probe atomic force microscopic approach for the characterization of the electrical heterogeneity of ITO/organic semiconductor interfaces on 20–500 nm length scales. This methodology should be applicable to the characterization of a wide range of heterojunctions between organic semiconductors and contact and interlayer materials relevant to thin film electronic technologies such as

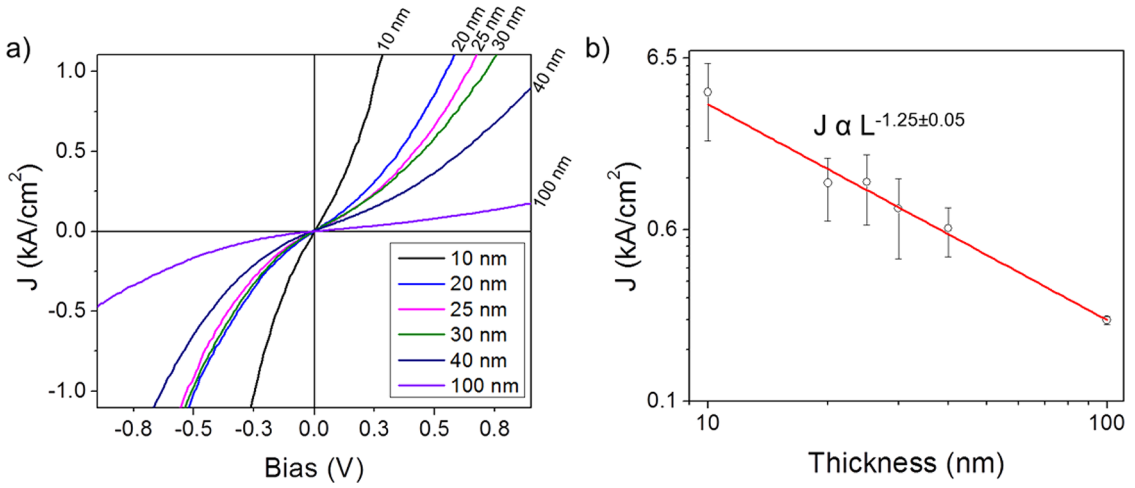

Figure 1. (a) *J*−*V* responses for 10, 20 25, 30, 40, and 100 nm CuPc thin films on a template-stripped gold substrate. These curves are an average of more than 75 *J*−*V* curves, obtained by taking 5 × 5 arrays with ~200 nm spacing at three or more locations spaced millimeters to centimeters from one another. (b) Absolute current *versus* film thickness at a bias of −300 mV, indicating that the *J*−*V* response is not limited by current injection (extraction) at either electrode for OPV relevant biases.

OPVs and OLEDs.[12,13,17,55,56] To demonstrate our approach, we characterize the interface between ITO and a prototypical donor organic semiconductor, copper phthalocyanine (CuPc), creating the lower half of a PHJ OPV.[57] The dependence of CuPc/C_{60} OPV performance on ITO pretreatments has been shown before, but not with submicrometer characterization of differences and distribution of the ohmic regions on the contacts.[57,58]

The worst performing ITO electrodes are cleaned by a combination of detergents and solvents (DSC-ITO), where previous C-AFM studies have shown that large fractions of the geometric area are incapable of passing measurable current densities, except at extremely high tip bias, confirmed by electrochemical studies of both solution and surface-confined redox probes.[18,19] As a control, we compare our results for CuPc/ITO heterojunctions to CuPc/Au heterojunctions, where the high work function of clean Au (*ca.* 5.1 eV) provides for an ohmic contact to CuPc thin films with an ionization potential (IP) of *ca.* 4.8 eV.[22,59] Similar behavior is seen for ITO electrodes first activated by oxygen plasma cleaning (OP-ITO) and by aggressive acid etching (AE-ITO).[18,19] Changes in electrical contact quality and the heterogeneity of the electroactivity in these heterojunctions are characterized as a function of ITO cleaning/activation procedure, which complements our previous C-AFM studies of ITO surfaces,[18,19] and as a function of small-molecule modification of the ITO surface with alkyl-phosphonic acids (PAs).[60,61] The electrical properties of this CuPc/ITO interface, and the heterogeneity therein, plays a critical role in power conversion efficiency of CuPc/C_{60} heterojunction OPVs, as has been predicted by other recent studies of contacts and electrical property heterogeneity in both small-molecule and polymer OPVs.[12,13,17,34,55,57,62,63]

We first demonstrate that the *J*−*V* response for CuPc on clean, high work function electrodes follows a non-field-dependent M−G model at the biases examined and is homogeneous as measured by SCS mapping. We next show a deviation away from ideal electrical behavior and an increase in heterogeneity for ITO electrodes that are not aggressively pretreated. The mapping of the nonidealities of these electrodes correlates well with previous studies that show that large areas of this TCO surface can be electroinactive[18,64] and with modeling studies from our group discussed elsewhere, which demonstrate the role of these heterogeneities in the efficiency of charge harvesting in OPV systems.[16,17] We anticipate that these findings will extrapolate to most OPV electrical contacts and that SCS mapping can provide a measure of contact quality on submicrometer length scales that correlates well with actual macroscopic OPV performance.

Lastly, these SCS maps are altered when the ITO electrode is modified with alkyl PA monolayers, which act as a uniform variable thickness insulating barrier to charge extraction (injection) between the electrode and the organic semiconductor and change both the chemical composition of the oxide surface and its effective work function.[61,65−67] For alkyl chain lengths of eight carbons or less the SCS electrical heterogeneity is reduced *versus* DSC-ITO alone, and OPV performance is actually comparable to that seen on OP-ITO. As alkyl chain length is increased above eight carbons, we observe a corresponding deviation from the M−G formalism in our maps, *i.e.*, the contact becomes more current limiting, in a controlled fashion. Such modifications lead to a systematic decrease in FF for CuPc/C_{60} OPV device performance, leading ultimately to the kind of S-shaped *J*−*V* behavior associated with enhanced recombination rates in poorly performing OPVs.[7,51]

RESULTS AND DISCUSSION

Current−Voltage Behavior in Au/CuPc Heterojunctions. We first show the *J*−*V* behavior of 10, 20 25, 30, 40,

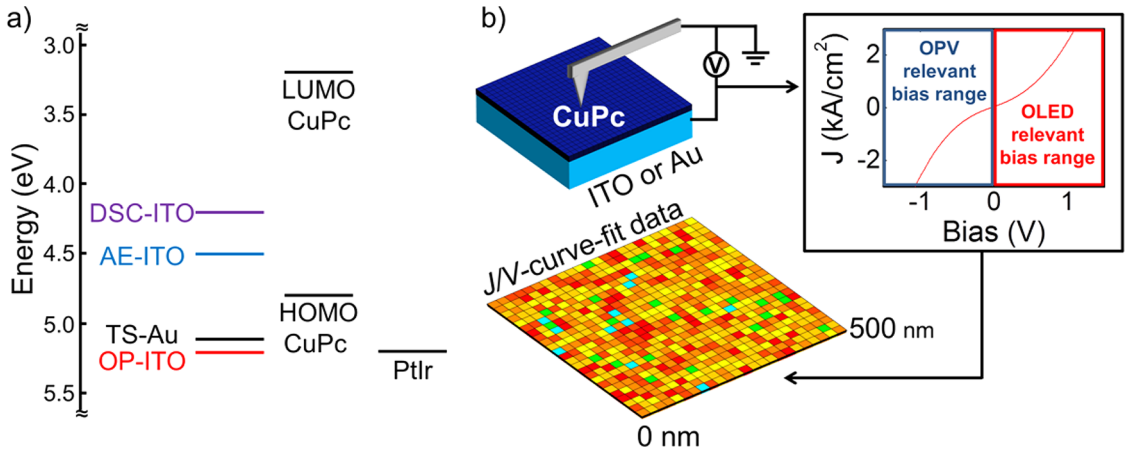

Figure 2. (a) Proposed band edge alignments for the ITO/CuPc/PtIr heterojunctions, assuming a pretreatment-dependent work function range for ITO of 4.2−5.2 eV (for DSC, AE-ITO, and OP-ITO), an IP/HOMO energy for CuPc of 4.8 eV, a LUMO of 3.2 eV, and a work function for the PtIr tip of 5.2 eV.[74] (b) Schematic representation of the SCS mapping experiment. *J*−*V* curves are collected from an array of spatially resolved points, with sampling dimensions of 500 × 500 nm and a point-to-point separation distance of 20 nm. From these individual *J*−*V* curves we extract the apparent hole mobility and the apparent power dependence of the current−voltage behavior. A power dependence that deviates from 2 indicates the presence of a nonohmic contact between the bottom electrode and the organic semiconductor.

and 100 nm CuPc thin films on TS-Au substrates (Figure 1a).[68,69] For these experiments the $PtIr_{05}$ probe is at ground and sample bias is swept positive or negative. At positive bias, holes are injected from the ITO electrode into the CuPc layer and extracted at the PtIr probe (*i.e.*, forward bias),[70−72] while at negative bias, holes are injected from the conductive probe into the CuPc film and extracted at the ITO electrode, a bias relevant to OPV operation. The *J*−*V* response for these TS-Au/CuPc heterojunctions represents an average of at least 75 *J*−*V* curves over a minimum of three distinct scan areas for each CuPc thickness.

As expected, the macroscopic *J*−*V* response for TS-Au/CuPc heterojunctions is uniformly ohmic; that is, the *J*−*V* behavior follows the M−G formalism (eq 1) for space-charge-limited current (SCLC) above a transition voltage.[21] A clear transition from an ohmic regime to SCLC, however, is not observed, which can be explained by two observations. First, for planar electrode/OSC/electrode geometries the transition voltage between the Ohm's law regime and the SCLC regime is expected to be less than 10 mV for most OSC films less than 100 nm thick.[21] A similar transition voltage can be expected for nanoscale *J*−*V* responses. Second, numerical modeling of C-AFM-based *J*−*V* measurements indicates that diffusion currents will have a significant contribution to the *J*−*V* response within the first few hundred millivolts, and this transition is strongly thickness dependent.[35] Thus the absence of a sharp transition between the Ohm's law regime and the SCLC regime is expected for OSC thin films of OPV-relevant thicknesses when characterized by C-AFM. In addition, the high work function of clean Au (5.1 eV)[73] and of the $PtIr_{05}$ tip (~5.2 eV)[74] *versus* the ionization potential of CuPc (*ca.* 4.8−5.2 eV)[22,59,75] produces no significant barrier to hole injection from either the $PtIr_{05}$ probe or the Au contact, the *J*−*V* response is not rectifying, ohmic responses are expected in both bias directions, and SCLC behavior is anticipated to dominate the *J*−*V* response.[21,50]

The thickness (*L*) dependence of current in this system at a constant bias (−300 mV) is shown in Figure 1b, showing $J \propto L^{-1.25\pm0.05}$, in good agreement with the experimental and modeled thickness dependence reported by Reid *et al.* ($I \propto L^{-1.4\pm1}$) for ITO/PEDOT:PSS/OSC heterojunctions.[35] Equation 1 typically applies to plane−plane electrodes of infinite size, showing a thickness dependence of L^{-3}. However, in these experiments the probe-OSC contact diameter (P_d) is similar in magnitude to the thickness of the OSC, where $P_d \approx 14$ nm.[35] As a result this system can be treated neither as having infinite plane−plane electrodes nor as a point−plane electrode system, but instead as an intermediate between these extremes. The electrode geometry-modified Mott−Gurney relationship proposed by Reid *et al.* (eq 2)[35] appears appropriate to describe the *J*−*V* properties of CuPc thin films using $PtIr_{05}$ conductive probes and is the response expected for ohmic, uniform contacts:

$$J = 8.2\varepsilon\varepsilon_o\mu\frac{V^2}{L^3}(7.8\pm1)\left(\frac{L}{P_d}\right)^{1.6\pm0.1} \quad (2)$$

The current densities, normalized to the expected tip/CuPc contact area, are in excess of 100 A/cm^2. Previous studies of small-area diode structures, however, have demonstrated that current densities in excess of 1000 A/cm^2 are achievable without damage to the organic layers.[76,77] Issues arising due to occasional $PtIr_{05}$ tip contamination, and remediation of those effects, are discussed further below. For a more detailed discussion of the steps taken to ensure good electrical contact between the probe and the OCS the reader is referred to the Supporting Information.

SCS Mapping of TS-Au/CuPc Heterojunctions and ITO/CuPc Heterojunctions As a Function of ITO Pretreatment. Figure 2a

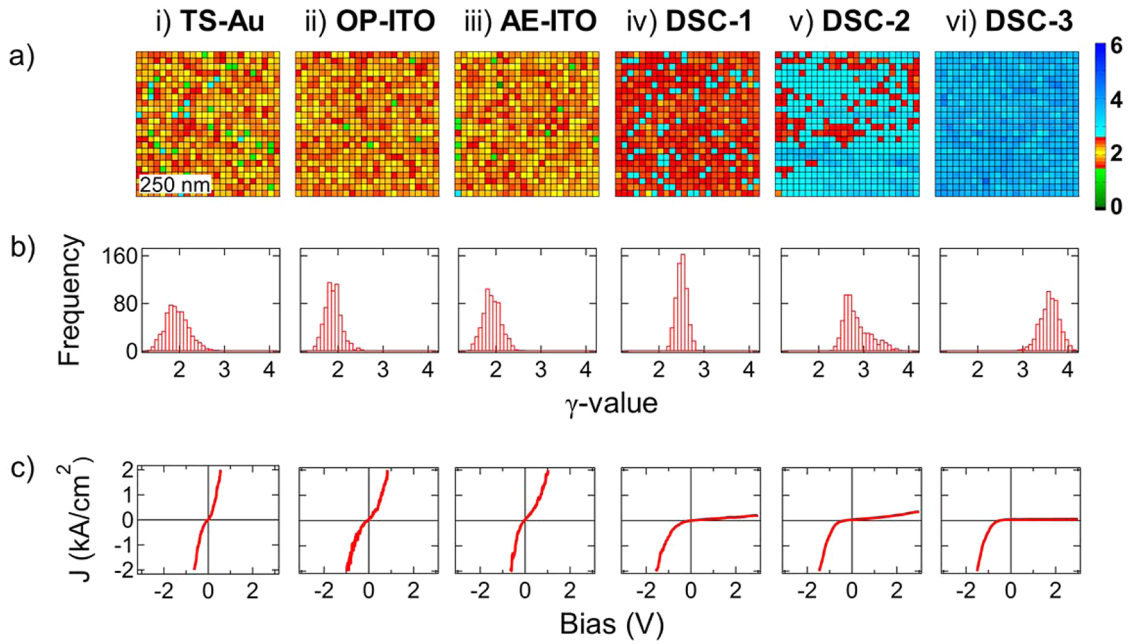

Figure 3. (a−c) Representative SCS data for 20 nm CuPC deposited on TS-Au, OP-ITO, and AE-ITO are presented in columns (i)−(iii), respectively. Columns (iv)−(vi) present SCS data for three distinct sample areas for CuPc/DSC-ITO, which show the typical variation observed between different samples and between different areas on the same sample for CuPC/DSC-ITO systems. Row (a) presents SCS maps, which demonstrate the variation in γ (Figure 3) for CuPc on TS-Au and ITO with various pretreatments. The datum value is represented by a color code: yellow indicates a value near 2 and transitions to red as the fitted value approaches $\pm 2.5\sigma$ from 2 relative to the model system CuPc/TS-Au. Green and cyan to blue indicate a deviation of greater than $\pm 2.5\sigma$ away from a power law of 2 and indicate a nonohmic contact. Row (b) shows the frequency distribution of γ in the above plots. Row (c) shows a representative $J-V$ curve taken from the above SCS mapping.

shows estimated frontier orbital energy (transport) levels for the CuPc HOMO and LUMO as well as the Fermi level for the $PtIr_{05}$ AFM probe and the Fermi level for the bottom contacts under investigation. These include TS-Au and ITO substrates pretreated by different protocols.[18,19] Figure 2b shows a schematic view of the SCS experiment, where we characterize the $J-V$ response for Au/CuPc/$PtIr_{05}$ and ITO/CuPc/$PtIr_{05}$ heterojunctions as a function of lateral displacement on a 500 × 500 nm^2 length scale.

Mapping of contact ohmicity was carried out by precisely positioning the $PtIr_{05}$ probe on the CuPc/contact, recording $J-V$ responses in both bias directions at each point. CuPc thicknesses of 20 nm were chosen for these mapping studies, which is near the optimal thicknesses for planar heterojunction CuPc/C_{60} OPVs.[30,57,59] Thinner and thicker CuPc films (10−100 nm) were also examined, with SCS mapping responses similar to those shown in Figure 3a. The $PtIr_{05}$ probe makes contact with the CuPc surface with only *ca.* 12 nN of force, with about 6 nN due to an instrumentally applied load, and the remainder is due to tip−sample adhesive forces. This force was chosen to avoid damaging the thin film and to minimize artifacts due to unknown contact area of the tip and tip-induced conductivity changes. Once the $J-V$ response was collected, the probe was withdrawn and moved a short distance (~20 nm) to collect another $J-V$ response. This process was repeated to produce a 25 × 25 array of $J-V$ curves over a 500 × 500 nm^2 area. A spacing of 20 nm between $J-V$ measurements was chosen, as this is near the theoretical limit for the resolution of this measurement for 20 nm thick CuPc films. On the basis of the numerical modeling done by Reid *et al.* ~91% of the current for this thickness should come from an area with a diameter of 24 nm and ~99% of the current should come from an area with a diameter of 36 nm based upon an isotropic OSC of uniform thickness, where these values correspond to 2σ and 3σ for the 2D Gaussian distribution of the electric field at the OSC ITO interface.

The $J-V$ data at each point was analyzed for both bias directions, but we focus here on the bias regime relevant to OPVs (hole injection from the $PtIr_{05}$ tip, through the CuPc layer with hole collection at the ITO substrate). The $J-V$ response at each position in the array was fit to a simplified power law expression (eq 3):

$$J = PV^{\gamma} \quad (3)$$

where P and γ represent a fitted prefactor (from eq 2) and fitted exponent, respectively.

For ohmic contacts the current, controlled by the electrical properties of the organic semiconductor, shows a $J \propto V^2$ dependence. Variations in the thicknesses of the organic layer and the tip contact area are expected only to change the magnitude of current at a given bias; we expect the fitted exponent γ to show little sensitivity to these variables, since γ reflects the charge transfer mechanism regardless of absolute current. However, large variations in the thickness could lead to cases where the magnitude of the current

falls outside of the detection window of the instrument in the bias range monitored or allows direct contact between the AFM probe and the bottom contact, often referred to as "shorts through pinholes" in the film. Such variations would deteriorate one's ability to obtain meaningful γ-fit values. The CuPc thin films investigated here tended to form crystals of ~20−40 nm range and with grain peak to grain boundary variation in height typically less than 3 nm for the 20 nm thick films. Large variations in the current were occasionally observed for CuPc films of 10−15 nm and often for films with thickness below 10 nm, both with SCS and traditional C-AFM imaging. CuPc films with a thickness of 20 nm and above showed no indication of pinholes. This correlates with the observation that films below this thickness perform suboptimally in OPVs.[57−59,64] For high-resolution topography images of ITO and ITO/CuPc systems the reader is referred to the Supporting Information.

If the contact is nonohmic, the current response is determined solely by the electrical properties of the ITO/CuPc heterojunction, through poor alignment of the critical energy levels between the electrode and the organic semiconductor, or through the presence of an insulating barrier at the ITO surface.[22,23,27] In the former case the current would be dictated by thermionic emission, and in the latter the current would be dictated by tunneling. In both these cases the $J-V$ response is expected to show an exponential dependence, *i.e.*, $\gamma \neq 2$. For convenience, we therefore use the fitted power, γ, as a figure of merit, where $\gamma \approx 2$ suggests an ohmic contact at that point on the sample. Large deviations from $\gamma = 2$ indicate either an energetic mismatch at that point or the presence of an insulating barrier of sufficient thickness to make the ITO/CuPc heterojunction current limiting. We note here that there is not a sharp distinction between bulk-limited and injection-limited currents; rather these represent cases when the charge transfer rate at the electrode interface is much greater than the transfer rate within the bulk (bulk limited) or much lower than the rate through the bulk (injection limited). In cases where these rates are similar in magnitude the current may be injection limited at low bias and bulk limited at high bias and have an intermediate response between these states at moderate bias.[50] We show below, however, that an ITO electrode with a sufficiently blocking layer (an alkyl-phosphonic acid) leads to an increasing deviation of γ away from 2, which correlates with an increasingly injection-limited contact.

There are clear differences in the SCS maps (Figure 3a), γ-fit distribution (Figure 3b), and $J-V$ response (Figure 3c) for CuPc heterojunctions on TS-Au, OP- and AE-ITO, and DSC-ITO (Figure 3 columns i, ii, iii, and iv−vi, respectively), where DSC-ITO produces the most variable electrical response. Figure 3c shows a representative $J-V$ for each electrode/CuPc system. The curve shape and magnitude are similar for CuPc on TS-Au, OP-ITO, and AE-ITO. For CuPc on DSC-ITO there is a decrease in both hole injection (positive bias) and extraction (negative bias) as well as a significant increase in rectification. We postulate that the work function of the DSC-ITO alone is not the sole cause for these changes, as we will demonstrate later in this communication, through alkylphosphonic acid modification of the ITO surface.

Yellow blocks in the SCS maps (Figure 3a) indicate a power law fit $\gamma \approx 2$, transitioning to red to represent γ as large as 2.5 and as small as 1.5 (value ranges of 2 ± 0.5 for the color code correspond with $\gamma \pm 2.5\sigma$ for CuPc on TS-Au). Figure 3b (i−vi) shows frequency distributions of the fitted power law dependence (γ) for representative 25 by 25 arrays for various TS-Au/ITO/CuPc heterojunctions. Distributions in γ centered around 2 for TS-Au/CuPc heterojunctions (*i*) and for OP-ITO/CuPc and AE-ITO/CuPc heterojunctions (*ii*, *iii*), with a standard deviation of 0.2. This represents the kind of deviation we expect for nominally ohmic TS-Au/CuPc heterojunctions.

We note that the typical grain size observed for the ITO substrates (Colorado Concepts) used in these experiments is ~50−100 nm. The scan size in all SCS measurements present in this communication is 500 × 500 nm. As a result, the SCS maps presented in Figure 3a (ii−vi) contain several ITO grains, ~25−50 grains per image, and a higher rms roughness (2−3 nm) than TS-Au (<1 nm). Despite the greater roughness and nanostructure variation of ITO compared to TS-Au, we observe a narrower distribution of γ on OP-ITO and AE-ITO than we observe for TS-Au (Figure 3b). From this we concluded that ITO nanostructure and variations in height in this range are not a primary factor in determining the quality of the SCS mapping at this time, although this could become a greater factor with further advances in this technique or for systems with greater surface roughness than what we observe here. High-resolution topography images of ITO and ITO/CuPc systems and information regarding the roughness of these systems can be found in the Supporting Information. During these control studies on Au/CuPc heterojunctions we noted occasional broadening of the distribution in values for γ, skewing of the distribution toward $\gamma \geq 2$, an increase in the adhesive forces between the probe and sample, as observed though force−distance curves, and a decrease in the coefficient of determination (R^2) for the fit of the experimental data to eq 3. We attributed these changes to contamination of the $PtIr_{05}$ tip and noted that replacement of the tip at this point returned the $J-V$ responses and the power law fit distributions to those expected for Au/CuPc heterojunctions. We therefore adopted these same cautionary measures in our exploration of all ITO/CuPc heterojunctions. A detailed description of how these tip effects were characterized and avoided and the criteria for acceptable $J-V$ behavior are discussed in the Supporting Information.

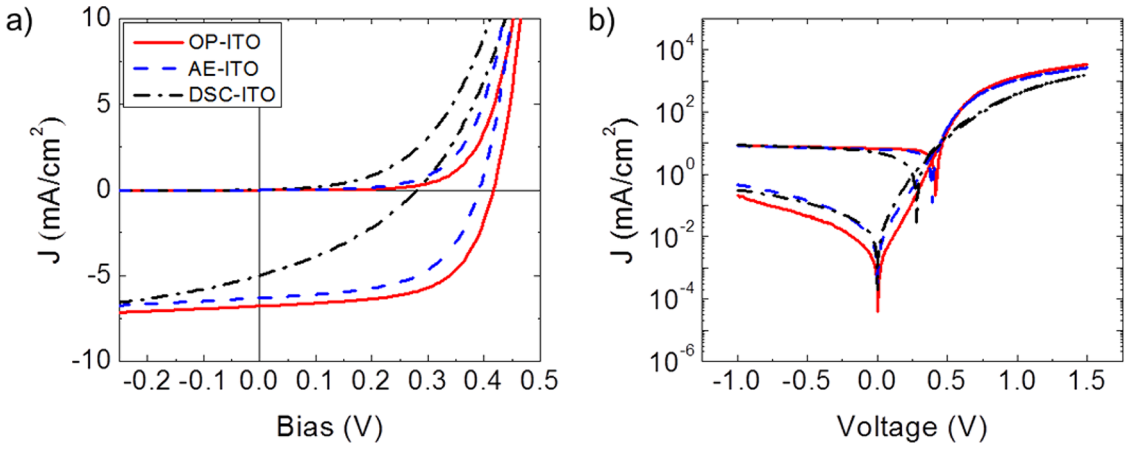

Figure 4. (a and b) Plots of light and dark $J-V$ curves for ITO/CuPc/C_{60}/BCP/Al OPVs as a function of ITO pretreatment, in linear−linear and semilog formats, respectively. DSC-ITO, with its high surface coverage of blocked sites, produces a response under illumination that suggests significant recombination limitations to the OPV response.[16,51,54]

TABLE 1. Summary of OPV Device Results for ITO/CuPc/C_{60}/BCP/Al Solar Cells As a Function of ITO Pretreatment Method[a]

	Φ (eV)	V_{OC} (V)	FF	J_{SC} (mA·cm^{-2})	R_S (Ω·cm)	η (%)
DSC-ITO	4.2 ± 0.1	0.28	0.34	4.9	0.8	0.48
AE-ITO	4.5 ± 0.1	0.39	0.57	6.3	0.44	1.41
OP-ITO	5.2 ± 0.1	0.42	0.61	6.8	0.33	1.7

[a] R_S was estimated from the slope of the dark $J-V$ response at far forward bias. Each reported measurement is the average of at least 10 separate determinations, with a standard deviation of typically less than 10%.

We observe $\gamma \approx 2$ for 20 nm CuPc on OP-ITO and AE-ITO (Figures 3b (ii and iii)). As expected, aggressive pretreatments allow for good electrical contact between the electrode and the CuPc thin film over 500 × 500 nm to millimeter length scales (spacing between unique areas on the same sample). The DSC-ITO/CuPc heterojunctions show significant deviations from $\gamma = 2$ for three different regions selected to show the range in electrical responses (Figure 3a (iv−vi)). Color bar values greater than 2.5 in these SCS maps are coded cyan to indicate significant deviation (>2.5σ) of γ away from the average values for TS-Au/CuPc heterojunctions, and color transitions for larger deviations ($\gamma = 6$) are coded in blue. This type of electrical heterogeneity, for a contact interfaced to a molecular semiconductor with relatively low charge mobility such as CuPc, has been predicted to lead to much higher rates of recombination in the OPV, increased series resistance (especially near the maximum power point in the OPV), lowered FF, and diminished OPV efficiency.[16,17,51]

OPV Device Performance: CuPc/C_{60} Heterojunctions. Figure 4 shows the averaged dark and illuminated $J-V$ responses for CuPc/C_{60} planar heterojunctions built on OP-ITO, AE-ITO, and DSC-ITO substrates; operating parameters are summarized in Table 1 from a minimum of 10 devices for each ITO pretreatment. V_{OC} and J_{SC} are nearly the same for OPVs on OP-ITO *versus* AE-ITO.[61,78] For the devices built on DSC-ITO the most significant differences are an increased R_S in the dark, significantly lowered FF, and much lower V_{OC}. It is notable that at large reverse bias the photocurrent for all three device types is nearly identical, suggesting that high internal fields in the OPV are sufficient to ensure efficient charge harvesting even for electrodes such as DSC-ITO, where large regions of the contact are "blocked".[12,13,16]

The macroscopic behavior of photovoltaic devices can be understood in terms of the SCS data. For both OP-ITO/CuPc and AE-ITO/CuPc heterojunctions we observe electrically homogeneous and ohmic behavior within 500 × 500 nm sample areas and between sample areas spaced micrometers to millimeters apart. CuPc films deposited on DSC-ITO showed a much greater variation in $J-V$ response and in the median and type of distribution observed for values of γ. The dramatic increase in R_S and reduction in FF and photocurrent response near V_{OC} for CuPc/C_{60} OPVs on DSC-ITO is correlated with this nonuniform and nonohmic electrical behavior. Such relationships have been inferred in the past, but without the accompanying SCS maps to verify this correlation.[30,57,58,79]

In a PHJ OPV operating near V_{OC}, photocreated charges arising at the CuPc/C_{60} interface move toward the contacts principally *via* diffusion.[31] In recent modeling studies we defined a characteristic diffusion length for charge carriers in a PHJ OPV (δ_{OPV}) and the average distance (d) separating individual electrically active sites at the contact surface. δ_{OPV} is determined both by linear diffusion of charges from the D/A interface and by the replenishment of these charges due to exciton dissociation and charge creation (under constant illumination) at the CuPc/C_{60} interface:

$$\delta_{OPV} = \frac{D}{\bar{V}} \quad (4)$$

For these OPVs we consider only D, the diffusion coefficient (cm^2/s), for a charge in the CuPc layer, which

is related to the hole mobility by the Einstein relation (*ca.* 2.9 × 10^{-4} $cm^2 \cdot V^{-1} \cdot s^{-1}$, leading to $D \approx 7.5 \times 10^{-6}$ $cm^2 \cdot s^{-1}$). $\bar{V}$ is the average velocity of a planar charge front incident perpendicular to the plane of the electrode. For CuPc/C_{60} OPVs operating near V_{OC} at AM1.5G illumination and light intensities up to 5× that level, we estimated $\bar{V}$ up to *ca.* 35 $cm \cdot s^{-1}$, leading to δ as small as *ca.* 200 nm. When electrostatic interactions between diffusing charge carriers in either the CuPc or C_{60} layers are considered, values of δ as low as *ca.* 20 nm are predicted.[16]

When $\delta_{OPV} \gg d$, no differences in charge collection efficiency are expected compared to the ideal homogeneous electrode; however, when δ_{OPV} is near or below the value for d, R_S is increased and the FF is decreased as charge harvesting is inhibited, and recombination probabilities near the contact or at the donor/acceptor interface in the OPV are enhanced.[12,13,16,17,51,79] For illustrative purposes we make the assumption that the areas coded yellow to red in Figure 3 are "unblocked", while the areas coded cyan to blue are "blocked", *i.e.*, injection limited. We acknowledge that this distinction can be somewhat arbitrary and discuss the limitations of these assumptions below.

For DSC-ITO we see the percentage of "electrically blocked areas" in our SCS maps is highly variable. Some sample areas, such as DSC-1 in Figure 3a, show a relatively low percentage of the surface to be electrically blocking. Areas such as DSC-2 show regions between tens and hundreds of nanometers that are highly blocked. Still other areas (DSC-3) show that the electrically blocking regions can be larger than 500 × 500 nm^2. We note that this range of results was repeatable over multiple experiments and multiple ITO samples and that the quality control measures described in the Supporting Information were implemented to minimize effects due to contamination of the AFM probe.

It is not surprising to see the poor CuPc/C_{60} OPV response for such ITO substrates relative to the activated ITO substrates, and it is surprising in some respects that the response is not worse. We have also noted, however, that once charges arrive at the ITO/CuPc interface under diffusion control (as is expected for OPVs operating near V_{OC}),[16,29,30] if they are not harvested at a blocked site, there are opportunities for lateral diffusion near the contact, dependent upon their charge mobilities in that interfacial region, and charges may still be efficiently harvested even with electrodes with high percentages of blocked areas.[16] For planar heterojunction OPVs based on donor layers such as pentacene, which has a significantly higher hole mobility than CuPc, we have observed that pentacene/C_{60} OPVs are much less sensitive to ITO activation conditions and that viable OPVs can be built even on DSC-ITO.[78] Results of these studies and comparisons with responses for other dipolar donor layers and for semiconducting polymer layers with higher hole mobilities will be communicated elsewhere.

While these modeling studies offer insight into the effect heterogeneity has on device performance, these systems tend to assume either blocked or nonblocked electrical behavior. In fact charge transfer at the electrode/OSC interface competes with the rates of intermolecular charge transfer, which control charge mobilities. Ohmic behavior is likely when interfacial charge harvesting rates are much higher than the intermolecular charge transfer rates, which control the charge mobility in the OSC. Nonohmic behavior is likely when interfacial charge harvesting rates are much slower than charge transfer rates within the OSC. As shown by Wang *et al.*, there is rarely a sharp distinction between these regimes, but rather a range of ohmic to nonohmic injection-limited behavior in most organic semiconductors.[50] Our approach to the analysis of $J-V$ behavior is intended to be comparative, emphasizing the major differences between ohmic and injection-limited regions.

Phosphonic Acid Modification of ITO Substrates. In the following section we discuss the use of alkyl-phosphonic acid modification of the ITO surface as an alternative approach to decrease the efficiency of hole harvesting at the ITO/CuPc interface. Although we did not observe a strong correlation between surface topography and SCS results for ITO cleaned by common pretreatments, literature precedent indicates that nanoscale surface curvature can detrimentally affect monolayer surface packing and increase defect densities.[80−83] To minimize this effect, we used ultrasmooth ITO (rms roughness <1 nm, Thin Film Devices) for all phosphonic acid modification experiments. This ITO maintains a high conductivity (∼20 Ω/□) but is much smoother, as does not contain the large grains (∼50−100 nm) that are observed on most commercially available ITO substrates. High-resolution topography images of ultrasmooth ITO and ITO/CuPc systems and information regarding the roughness of these systems can be found in the Supporting Information. The alkyl-PA chain lengths explored varied from 6 to 18 carbons, making the contact systematically more injection limiting as the alkyl chain length increased. PA modifiers bind robustly to activated ITO surfaces, and terminal functional groups can introduce dipolar character that can be used to tune the effective work function of the ITO substrate.[65−67] Using simple alkyl-PAs, the work function of ITO is lowered, relative to OP-ITO, and the thickness of the insulating layer is systematically increased as chain length is increased. Alkyl-phosphonic acid modification of ITO, with chain lengths between 6 and 18 carbons, have been shown to produce substrates with work functions nearly the same as DSC-ITO.[61]

Current flux through an insulating barrier is exponentially dependent on applied bias, while current through an organic semiconductor has a quadratic bias dependence.[84,85] It has been shown that the

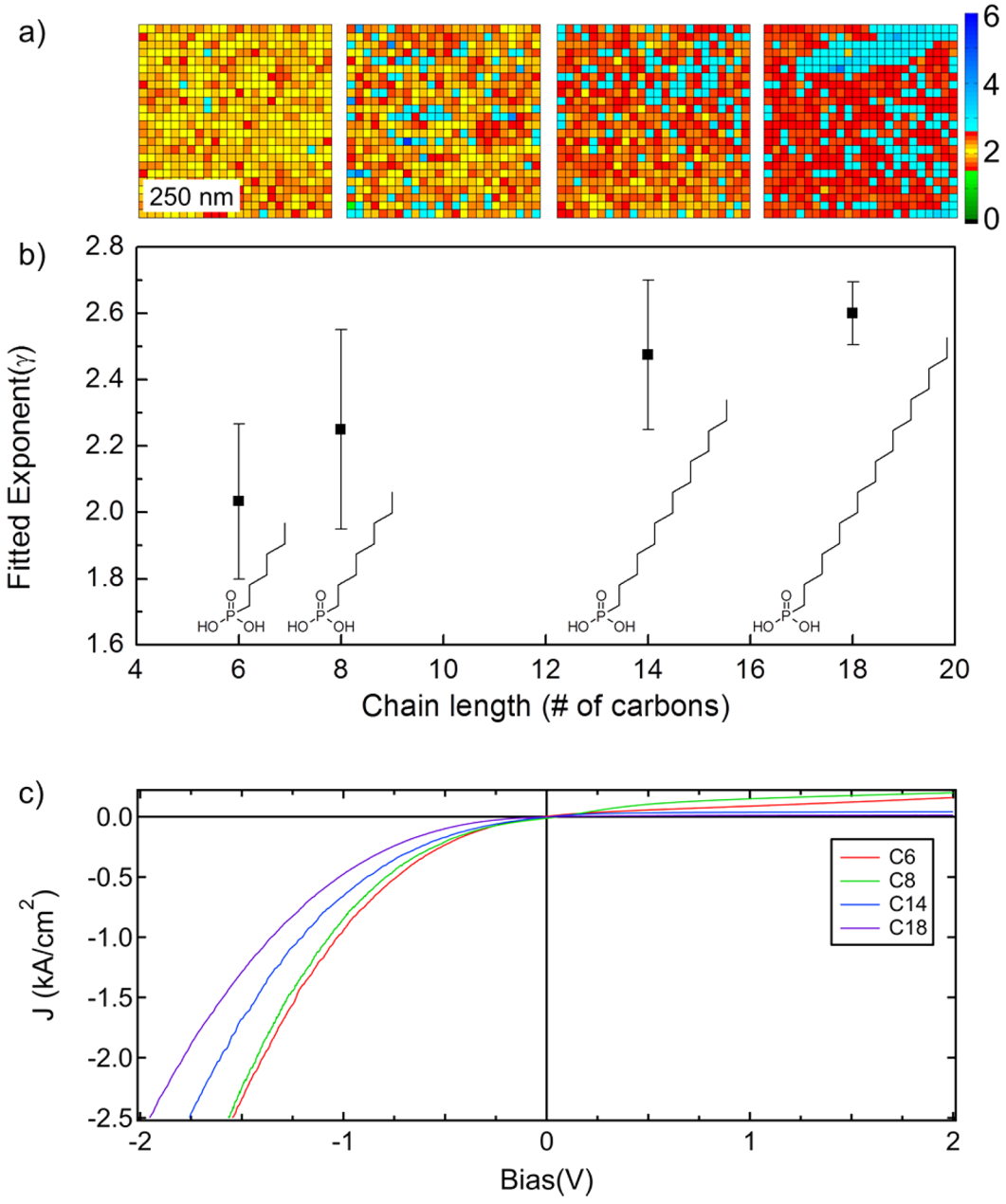

Figure 5. (a) The 500 × 500 nm surface plots showing the *x*−*y* distribution of power law fits for 20 nm CuPc on ITO modified with 6-, 8-, 14-, and 18-carbon alkyl-phosphonic acid monolayers (negative bias). (b) Fitted exponent (γ) in the power law dependence for all of the *J*−*V* curves used to make up the maps above, showing the average value of the exponent and standard deviation for 20 nm of CuPc on gold, and PA-modified modified ITO with alkyl chain lengths of 6, 8, 14, and 18 carbons. (c) *J*−*V* responses for PA-ITO/CuPc heterojunctions averaged over full SCS mapping area presented in (a).

tunneling efficiency through alkylthiol monolayers on gold has an exponential dependence on the alkyl chain length.[86] An asymptotic transition from injection-limited current responses to bulk-limited current responses is expected as the bias is increased. ITO/PA/CuPc heterojunctions based on short alkyl-PA groups were expected to transition to bulk-limited currents at lower voltages than ITO/PA/CuPc heterojunctions based on longer alkyl-PA chains, demonstrating *J*−*V* responses closely resembling systems with ohmic contacts.

Figure 5c shows that the *J*−*V* behavior of ITO-PA/CuPc heterojunctions is rectifying in the same manner seen for DSC-ITO/CuPc heterojunctions and that the ohmicity of the contact for ITO/PA/CuPc heterojunctions varies monotonically with PA alkyl chain length. Figure 5a shows representative surface plots of the γ power law fit for ITO/PA/CuPc heterojunctions modified with PA alkyl chain lengths of 6, 8, 14, and 18 carbons, increasing from left to right. Figure 5b shows γ values, from the negative bias regime, averaged over multiple areas, plotted against PA alkyl chain length. ITO/PA/CuPc heterojunctions with C6- and C8-PAs show γ values close to those seen for Au/CuPc and OP-ITO/CuPc heterojunctions, after accounting for the

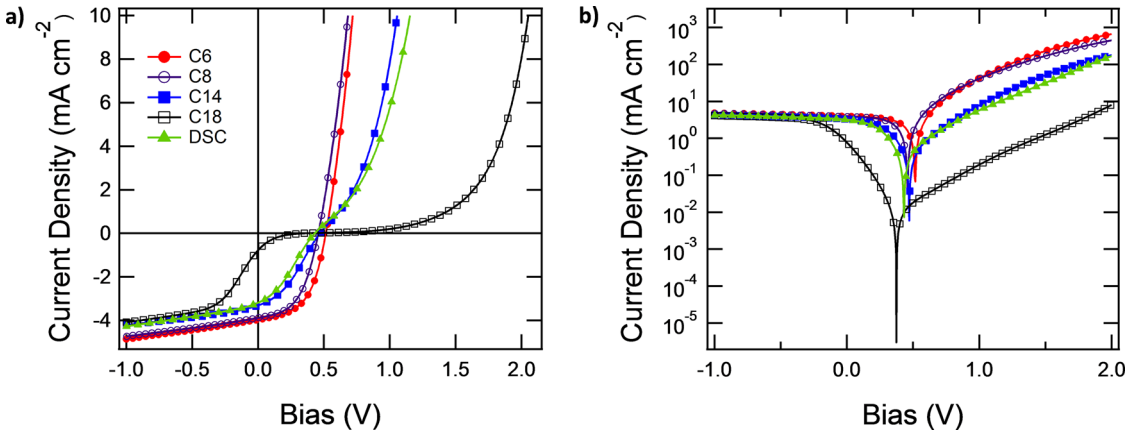

Figure 6. (a and b) Linear−linear and log−linear, light *J*−*V* curves (see SI for dark JV curves) for ITO/CuPc/C_{60}/BCP/Al OPVs as a function alkyl-PA modification of ITO, respectively. For the C6- and C8-PA chain lengths the OPV response is not significantly different from that seen for OP-ITO (Figure 4), while for C14 the OPV response is similar to that seen for DSC-ITO. For C18 PA modification the *J*−*V* response is significantly compromised, as shown in Figure 5, and the OPV response is clearly recombination limited.[51,54]

TABLE 2. Summary of OPV Device Results for ITO/CuPc/C_{60}/BCP/Al Solar Cells As a Function of ITO Pretreatment Method[a]

	V_{OC} (V)	J_{SC} (mA·cm^{-2})	FF	R_S (Ω·cm^2)	η (%)
C6	0.52	−4.0	0.53	0.38	1.1
C8	0.47	−3.9	0.49	0.52	0.9
C14	0.48	−3.3	0.34	0.5	0.5
C18	0.37	−0.8	0.10	0.9	0.03
DSC	0.41	−3.2	0.33	0.5	0.4
control	0.49	−3.6	0.54	1.0	1.0

[a] R_S was estimated from the slope at 2.95 V. Each reported measurement is the average of at least 10 separate determinations, with a standard deviation of typically less than 10%. The control sample was OP-ITO soaked in pure ethanol.

precision of the measurement. Values for γ are 2.5 ± 0.2 and 2.6 ± 0.1 for C14- and C18-PAs, respectively. Since we expect an exponential dependence of the current relative to the voltage for charge transport through an insulating barrier, the apparent γ value will depend on bias voltage window for such nonohmic contacts. In contrast, the response of ohmic contacts is bias-window independent before electrical breakdown; thus comparisons of ITO electrodes modified with variable chain length PAs should be viewed as semiquantitative. This approach, however, still allows the extraction of meaningful average values of γ for SCS mapping of the modified contact and preserves the lateral resolution that is lost when *J*−*V* curves are averaged without regard to spatial distribution of the measurements.

We note that ITO substrates modified with C6- or C8-PAs show largely homogeneous and ohmic SCS maps. The C6-PA-modified surface shows a similar response to that seen for OP-ITO, both with $\gamma \approx 2$; however the average current density at −1 V is approximately twice as large for CuPc on TS-Au than on C6-PA-ITO. This indicates that C6-PA modification of the surface leads to a contact that is less ohmic to CuPc than TS-Au, but is indistinguishable based on values of γ alone. As the chain length increases, the current density decreases even further and γ values increase. For C14-PA-modified ITO the separation between sites exhibiting γ values of 2 have increased to greater than 60 nm in some areas. The fact that there are sites demonstrating nearly ohmic responses is likely due to the intrinsic disorder in these self-assembled monolayers, as well as the experimental error in the measurement.[18,61,65] For C18-PA modified ITO less than *ca.* 1% of the ITO geometric area exhibits ohmic behavior, suggesting significant deterioration in OPV response for CuPc/C_{60} heterojunctions deposited on these modified substrates. For C18-PA-modified ITO we often observed distinct regions of lower ohmicity, as can be seen in Figure 5a for the SCS mapping of CuPc on C18-PA-modified ITO. It is possible that regions like this are due to the formation of adlayers beyond the first monolayer, due to the lower solubility of octadecylphosphonic acid in ethanol than that of the other PA modifiers. Alternatively this could be due to regions where a denser, less defective monolayer is achieved. With this system we are unable to distinguish between these possibilities, as both are expected to lead to height variations of less than 1 nm. However, after CuPc deposition the rms roughness increased to ~3 nm. This level of roughness does not allow for us to differentiate between the above possibilities, as both are expected to lead to height variation of less than the peak to valley variation observed for ITO/CuPc alone. More information about the topography of ITO/CuPc systems can be found in the Supporting Information.

CuPc/C_{60} OPVs on PA-ITO Substrates. Figure 6 shows the *J*−*V* response for CuPc/C_{60} OPVs, under illumination, deposited on PA-modified ITO using 6-, 8-, 14-, and 18-carbon alkyl-PAs and on an identically treated "control" ITO sample soaked only in pure ethanol. Dark *J*−*V* curves have been omitted for clarity and can be found in the Supporting Information. Table 2 summarizes these results. Fill factors at or above 0.5 were measured for devices built on C6- and C8-modified ITO. R_S, estimated at far forward bias (*ca.* 3 V), for devices built

on C6-PA-ITO and C8-PA-ITO were 0.4 and 0.5 $\Omega \cdot cm^2$, respectively, correlating with the nearly ohmic responses seen in our C-AFM and SCS mapping experiments.

Devices built on C14-PA-ITO demonstrated a "kink" in the illuminated $J-V$ response corresponding to enhanced recombination near V_{OC}, leading to a significantly lower FF of 0.34 $\pm$ 0.04 and decreased efficiency, even though the measured R_S is similar to that observed for devices built on C8-PA-ITO (Table 2). OPV performance for this modified ITO substrate was comparable to that seen for CuPc/C_{60} heterojunctions on DSC-ITO. The electrical heterogeneity we have observed for DSC-ITO systems is much greater than that observed for C14-PA-ITO. We speculate that the additional heterogeneity, as observed in SCS mapping, may have a detrimental effect on device lifetime relative to the C14-modified system since the current flux is expected to be concentrated in the areas with better electrical contact, which may increase local joule heating in these areas, accelerating degradation. CuPc/C_{60} OPVs on C18-PA-ITO demonstrated even more recombination-limited $J-V$ behavior with saturation photocurrent observable only at far negative bias. For these devices R_S was nearly 2$\times$ that seen for the other devices. It has been shown that tunneling efficiencies through alkylthiol monolayers decrease exponentially with increasing chain length,[86] and it is not surprising to see such recombination-limited behavior on such significantly modified contacts.[51,54]

CONCLUSIONS

We have demonstrated a new and convenient approach to the mapping of electrical activity of OPV-relevant interfaces between organic semiconductors and ITO on submicrometer to nanometer length scales. This method is expected to extrapolate to a wide range of contacts and interlayer materials for thin film PV technologies, beyond OPVs. By careful acquisition of $J-V$ responses with sub-100 nm lateral resolution we are able to estimate the degree of ohmicity of each site and estimate the average separation distance between those sites as might be relevant for charge collection in a thin film PV. Activation of the ITO surface with oxygen plasma and/or brief exposure to strong acids is well established as a route to creating a more ohmic contact to organic semiconductors such as CuPc,[18,19] and interestingly even chemical modification of the ITO surface with a short-chain PA produces a more uniform and ohmic response, with good OPV efficiencies relative to detergent/solvent cleaning alone. Presumably the PA modification step produces a stable, low-energy surface, preventing the buildup of an additional contamination layer, and the charge harvesting through this insulating layer is sufficiently efficient that device performance is minimally impacted. CuPc/C_{60} PHJ OPVs present a significant challenge to these substrates because the low hole mobility in CuPc films requires that ohmic regions be spaced no farther apart than *ca.* 200 nm so that efficient harvesting of diffusing photogenerated charges occurs (operating at AM 1.5 illumination conditions, near V_{OC}). For organic semiconductor small-molecule and polymer layers with much higher charge mobilities the critical separation distance between ohmic sites is likely to be relaxed. As an example, nearly ideal OPV behavior has been observed for planar pentacene/C_{60} heterojunctions whether devices used DSC-ITO substrates or a variety of ITO substrates modified with both alkyl- and benzylphosphonic acids.[78] In work to be reported elsewhere we also show that ITO contact ohmicity is even more important when the donor layer in the OPV interacts strongly with the oxide surface, implying that charge transfer to ITO in that case requires a specific molecular orientation over the active site on the oxide surface. For polymer donor layers created from strongly dipolar subunits and/or where interactions between the donor polymer and the contact alter the in-plane charge mobilities, it is anticipated that electrical heterogeneity in the contact may play a key role in the overall device efficiency.

EXPERIMENTAL SECTION

ITO films on glass for some of the SCS and OPV studies were obtained from Colorado Concepts Coatings LLC, whereas ITO from Thin Film Devices Inc. was used for studies of ITO modification with PAs. All ITO samples were hand cut, then cleaned by rinsing with water, then scrubbing with microfiber cloths (Peca Products Inc. ST-1) and Triton X-100 detergent (Alfa-Aesar), followed by rinsing in water and sonication in dilute Triton X-100 for 10 min. The samples were then rinsed three times and sonicated 10 min in Millipore water, followed by rinsing three times and sonication for 10 min in absolute ethanol (Decon Laboratories). These "DSC-ITO" samples were then blown dry with compressed nitrogen prior to use. DSC-ITO samples that were subsequently oxygen plasma treated in a Harrick PDC-32G plasma cleaner for 8.5 min on medium power (10.5 W) in a 300 mTorr oxygen environment are referred to as "OP-ITO".[18] ITO that was acid etched by flooding the surface for *ca.* 10 s in a 0.2 M solution of $FeCl_3$ (EMD Chemicals Inc.) in concentrated HCl (EMD Chemicals Inc.) is referred to as "AE-ITO". The acid etching was immediately followed by copious rinsing in Millipore water and blowing dry with nitrogen.

For phosphonic acid modification OP-ITO was immersed in a solution of 10 mM phoshonic acid in ethanol (or for control samples, soaked in pure ethanol), as discussed elsewhere.[60,61] Substrates were soaked a minimum of 12 h followed by an anneal at 120 °C for a minimum of 12 h. Substrates were then rinsed three times with absolute ethanol and sonicated for 10 min in a 5% v/v solution of triethyl amine/ethanol solution.[60,61] Substratates were then rinsed three times in absolute ethanol and dried in a nitrogen stream.

Copper phthalocyanine (Alfa Aesar), C_{60} fullerene (Materials and Electrochemical Research Corp.), and bathocuproine (Sigma Aldrich) were purified by triple sublimation and then deposited by physical vapor deposition from Knudsen cell sources at a

pressure of *ca.* 5×10^{-7} Torr and a rate of *ca.* 1 Å·s^{-1}. Film thickness was monitored by a quartz crystal oscillator.[59] Aluminum cathodes were deposited by physical vapor deposition from alumina-coated tungsten boats (Kurt J. Lesker) at a rate of 0.7−1.5 Å·s^{-1}. The device structures were 20 nm CuPc/40 nm C_{60}/10 nm BCP/100 nm Al. OPVs were tested in a nitrogen glovebox, under illumination from a tungsten lamp. *J*−*V* curves were measured with a Keithley 2400 source meter.

Template-stripped gold (rms roughness less than 1 nm detemined by AFM) was fabricated by thermal evaporation of 100 nm of gold (Kurt J. Lesker) onto silicon substrates (Silicon Quest International, item #707-005). Glass substrates were adhered to gold with epoxy (Epoxy Technology, EPO-TEK 353ND4), followed by an overnight 120 °C anneal in an oven. A razor blade was run around the perimeter of the glass substrate prior to removal from the silicon substrate. TS-Au substrates were oxygen plasma treated in a Harrick PDC-32G plasma cleaner for 8.5 min on medium power (10.5 W) in a 300 mTorr oxygen environment immediatly prior to loading in a vacuum chamber for CuPc deposition.

C-AFM measurements were made using a Dimension 3100 AFM with a Nanoscope IV controller and extended TUNA module from Veeco Instruments. Measurements were performed both in ambient and in an argon-purged drybox. SCS measurements for CuPc films were qualitatively the same with and without an inert argon environment. Contact mode images and electrical measurements were made using Veeco SCM-PIC platinum−iridium alloy coated probes with a 0.2 N/m nominal spring constant. Silver paint (Ted Pella Leitsilber 200) was used to make electrical contact between the sample and the AFM's vacuum chuck. Next, a force curve was obtained and the sample engagement set-point adjusted to provide a 32 nm cantilever deflection, corresponding to a tip−surface force of ∼6.4 nN. The "Ramp Channel" was changed to "Sample Bias". This allows the AFM software to obtain current−voltage curves. For CuPc films on TS-Au, OP-ITO, and AE-ITO a voltage range of −2 to 2 V with either 256 or 512 data points per curve was used, at a rate of 0.5 Hz. DSC-ITO required a larger voltage sweep, −4 to 4 V, to obtain similar currents. All phosphonic acid-modified samples were characterized with a bias range of −2.5 to 2 V. Once the proper current amplifier and scan settings were found, the "Scan Array" function was used to obtain an array of current−voltage curves evenly spaced over the area of interest. In this mode the Nanoscope 5.31R1 software lifts the tip off of the surface before moving to a new position, protecting the tip and surface from damage. The data for this work consisted of 25 × 25 point arrays, with a spacing of 20 nm. A Matlab program imported the individual data files and sorted them into a cell array. Each individual current−voltage curve was fit to an appropriate equation (see descriptions below), and the fitted parameters were stored in separate matrices. Data below 500 mV, in absolute magnitude, were excluded from the curve fitting since the current due to lateral diffusion of charge carriers contributes an increasing proportion of the total current as the applied bias approaches zero.[35]

Conflict of Interest: The authors declare no competing financial interest.

Acknowledgment. This work was supported as part of the Center for Interface Science: Solar Electric Materials, an Energy Frontier Research Center funded by the U.S. Department of Energy, Office of Science, Office of Basic Energy Sciences, under Award Number DE-SC0001084.

Supporting Information Available: Discussion of the quality control methods used to ensure reliability of nanoscale *J*−*V* measurements, as well as dark *J*−*V* curves from Figure 5, and high-resolution topographic images of bare ITO and CuPc-coated ITO substrates are available free of charge *via* the Internet at http://pubs.acs.org.

REFERENCES AND NOTES

1. Brabec, C. J.; Gowrisanker, S.; Halls, J. J. M.; Laird, D.; Jia, S. J.; Williams, S. P. Polymer-Fullerene Bulk-Heterojunction Solar Cells. *Adv. Mater.* **2010**, *22*, 3839–3856.
2. Steim, R.; Ameri, T.; Schilinsky, P.; Waldauf, C.; Dennler, G.; Scharber, M.; Brabec, C. J. Organic Photovoltaics for Low Light Applications. *Sol. Energy Mater. Sol. Cells* **2011**, *95*, 3256–3261.
3. Gong, X.; Tong, M. H.; Brunetti, F. G.; Seo, J.; Sun, Y. M.; Moses, D.; Wudl, F.; Heeger, A. J. Bulk Heterojunction Solar Cells with Large Open-Circuit Voltage: Electron Transfer with Small Donor-Acceptor Energy Offset. *Adv. Mater.* **2011**, *23*, 2272−+.
4. Sun, Y.; Welch, G. C.; Leong, W. L.; Takacs, C. J.; Bazan, G. C.; Heeger, A. J. Solution-Processed Small-Molecule Solar Cells with 6.7% Efficiency. *Nat. Mater.* **2012**, *11*, 44–48.
5. Riede, M.; Uhrich, C.; Widmer, J.; Timmreck, R.; Wynands, D.; Schwartz, G.; Gnehr, W. M.; Hildebrandt, D.; Weiss, A.; Hwang, J.; *et al.* Efficient Organic Tandem Solar Cells Based on Small Molecules. *Adv. Funct. Mater.* **2011**, *21*, 3019–3028.
6. Meiss, J.; Menke, T.; Leo, K.; Uhrich, C.; Gnehr, W. M.; Sonntag, S.; Pfeiffer, M.; Riede, M. Highly Efficient Semitransparent Tandem Organic Solar Cells with Complementary Absorber Materials. *Appl. Phys. Lett.* **2012**, *100*, 099901.
7. Tress, W.; Leo, K.; Riede, M. Optimum Mobility, Contact Properties, and Open-Circuit Voltage of Organic Solar Cells: A Drift-Diffusion Simulation Study. *Phys. Rev. B* **2012**, *85*.
8. Cai, N.; Moon, S. J.; Cevey-Ha, L.; Moehl, T.; Humphry-Baker, R.; Wang, P.; Zakeeruddin, S. M.; Gratzel, M. An Organic D-π-A Dye for Record Efficiency Solid-State Sensitized Heterojunction Solar Cells. *Nano Lett.* **2011**, *11*, 1452–1456.
9. Morgenstern, F. S. F.; Kabra, D.; Massip, S.; Brenner, T. J. K.; Lyons, P. E.; Coleman, J. N.; Friend, R. H. Ag-Nanowire Films Coated with Zno Nanoparticles as a Transparent Electrode for Solar Cells. *Appl. Phys. Lett.* **2011**, *99*, 183307.
10. Gaynor, W.; Lee, J. Y.; Peumans, P. Fully Solution-Processed Inverted Polymer Solar Cells with Laminated Nanowire Electrodes. *ACS Nano* **2010**, *4*, 30–34.
11. Seungkeun, C.; Potscavage, W. J., Jr.; Bernard, K. Area-Scaling of Organic Solar Cells. *J. Appl. Phys.* **2009**, *106*, 054507.
12. Steim, R.; Kogler, F. R.; Brabec, C. J. Interface Materials for Organic Solar Cells. *J. Mater. Chem.* **2010**, *20*, 2499–2512.
13. Steim, R.; Choulis, S. A.; Schilinsky, P.; Lemmer, U.; Brabec, C. J. Formation and Impact of Hot Spots on the Performance of Organic Photovoltaic Cells. *Appl. Phys. Lett.* **2009**, *94*, 043304.
14. Krebs, F. C. Roll-to-Roll Fabrication of Monolithic Large-Area Polymer Solar Cells Free from Indium-Tin-Oxide. *Sol. Energy Mater. Sol. Cells* **2009**, *93*, 1636–1641.
15. Tvingstedt, K.; Inganas, O. Electrode Grids for ITO-Free Organic Photovoltaic Devices. *Adv. Mater.* **2007**, *19*, 2893–2897.
16. Zacher, B.; Armstrong, N. R. Modeling the Effects of Molecular Length Scale Electrode Heterogeneity in Organic Solar Cells. *J. Phys. Chem. C* **2011**, *115*, 25496–25507.
17. Ratcliff, E. L.; Zacher, B.; Armstrong, N. R. Selective Interlayers and Contacts in Organic Photovoltaic Cells. *J. Phys. Chem. Lett.* **2011**, 1337–1350.
18. Brumbach, M.; Veneman, P. A.; Marrikar, F. S.; Schulmeyer, T.; Simmonds, A.; Xia, W.; Lee, P. A.; Armstrong, N. R. Surface Composition and Electrical and Electrochemical Properties of Freshly Deposited and Acid-Etched Indium Tin Oxide Electrodes. *Langmuir* **2007**, *23*, 11089–11099.
19. Armstrong, N. R.; Veneman, P. A.; Ratcliff, E.; Placencia, D.; Brumbach, M. Oxide Contacts in Organic Photovoltaics: Characterization and Control of Near-Surface Composition in Indium-Tin Oxide (ITO) Electrodes. *Acc. Chem. Res.* **2009**, *42*, 1748–1757.
20. Petersen, A.; Kirchartz, T.; Wagner, T. A. Charge Extraction and Photocurrent in Organic Bulk Heterojunction Solar Cells. *Phys. Rev. B* **2012**, *85*.
21. Shen, Y. L.; Hosseini, A. R.; Wong, M. H.; Malliaras, G. G. How to Make Ohmic Contacts to Organic Semiconductors. *ChemPhysChem* **2004**, *5*, 16–25.

22. Hwang, J.; Wan, A.; Kahn, A. Energetics of Metal-Organic Interfaces: New Experiments and Assessment of the Field. *Mat. Sci. Eng. R* **2009**, *64*, 1–31.
23. Fong, H. H.; Papadimitratos, A.; Hwang, J.; Kahn, A.; Malliaras, G. G. Hole Injection in a Model Fluorene-Triarylamine Copolymer. *Adv. Funct. Mater.* **2009**, *19*, 304–310.
24. Salomon, A.; Boecking, T.; Seitz, O.; Markus, T.; Amy, F.; Chan, C.; Zhao, W.; Cahen, D.; Kahn, A. What Is the Barrier for Tunneling through Alkyl Monolayers? Results from N- and P-Si-Alkyl/Hg Junctions. *Adv. Mater.* **2007**, *19*, 445–+.
25. Peisert, H.; Petr, A.; Dunsch, L.; Chasse, T.; Knupfer, M. Interface Fermi Level Pinning at Contacts between Pedot: Pss and Molecular Organic Semiconductors. *ChemPhysChem* **2007**, *8*, 386–390.
26. Kim, J. S.; Cacialli, F.; Friend, R. Surface Conditioning of Indium-Tin Oxide Anodes for Organic Light-Emitting Diodes. *Thin Solid Films* **2003**, *445*, 358–366.
27. Liau, Y. H.; Scherer, N. F.; Rhodes, K. Nanoscale Electrical Conductivity and Surface Spectroscopic Studies of Indium-Tin Oxide. *J. Phys. Chem. B* **2001**, *105*, 3282–3288.
28. Shen, Y.; Klein, M. W.; Jacobs, D. B.; Campbell Scott, J.; Malliaras, G. G. Mobility-Dependent Charge Injection into an Organic Semiconductor. *Phys. Rev. Lett.* **2001**, *86*, 3867–3870.
29. Giebink, N. C.; Wiederrecht, G. P.; Wasielewski, M. R.; Forrest, S. R. Ideal Diode Equation for Organic Heterojunctions. I. Derivation and Application. *Phys. Rev. B* **2010**, *82*.
30. Forrest, S. R. The Limits to Organic Photovoltaic Cell Efficiency. *MRS Bull.* **2005**, *30*, 28–32.
31. Gregg, B. A.; Hanna, M. C. Comparing Organic to Inorganic Photovoltaic Cells: Theory, Experiment, and Simulation. *J. Appl. Phys.* **2003**, *93*, 3605–3614.
32. van der Heide, A. S. H.; Schonecker, A.; Bultman, J. H.; Sinke, W. C. Explanation of High Solar Cell Diode Factors by Nonuniform Contact Resistance. *Progr. Photovoltaics* **2005**, *13*, 3–16.
33. Sullivan, J. P.; Tung, R. T.; Pinto, M. R.; Graham, W. R. Electron-Transport of Inhomogeneous Schottky Barriers - a Numerical Study. *J. Appl. Phys.* **1991**, *70*, 7403–7424.
34. Pingree, L. S. C.; Reid, O. G.; Ginger, D. S. Imaging the Evolution of Nanoscale Photocurrent Collection and Transport Networks During Annealing of Polythiophene/Fullerene Solar Cells. *Nano Lett.* **2009**, *9*, 2946–2952.
35. Reid, O. G.; Munechika, K.; Ginger, D. S. Space Charge Limited Current Measurements on Conjugated Polymer Films Using Conductive Atomic Force Microscopy. *Nano Lett.* **2008**, *8*, 1602–1609.
36. Loiacono, M. J.; Granstrom, E. L.; Frisbie, C. D. Investigation of Charge Transport in Thin, Doped Sexithiophene Crystals by Conducting Probe Atomic Force Microscopy. *J. Phys. Chem. B* **1998**, *102*, 1679–1688.
37. Lin, H. N.; Chen, S. H.; Perng, G. Y.; Chen, S. A. Nanoscale Surface Electrical Properties of Indium-Tin-Oxide Films for Organic Light Emitting Diodes Investigated by Conducting Atomic Force Microscopy. *J. Appl. Phys.* **2001**, *89*, 3976–3979.
38. Alexeev, A.; Loos, J.; Koetse, M. M. Nanoscale Electrical Characterization of Semiconducting Polymer Blends by Conductive Atomic Force Microscopy. *Ultramicroscopy* **2006**, *106*, 191–199.
39. Matz, D. L.; Pemberton, J. E. Reaction Chemistry of Solid-State Pyridine Thin Films with Vapor Deposited Ag, Mg, and Al. *J. Phys. Chem. C* **2012**.
40. Schalnat, M. C.; Hawkridge, A. M.; Pemberton, J. E. Raman Spectroscopy of the Reaction of Thin Films of Solid-State Benzene with Vapor-Deposited Ag, Mg, and Al. *J. Phys. Chem. C* **2011**, *115*, 13717–13724.
41. Bietsch, A. Electrical Testing of Gold Nanostructures by Conducting Atomic Force Microscopy. *J. Vac. Sci. Technol. B* **2000**, *18*, 1160.
42. Frazzetto, A.; Giannazzo, F.; Lo Nigro, R.; Di Franco, S.; Bongiorno, C.; Saggio, M.; Zanetti, E.; Raineri, V.; Roccaforte, F.: Nanoscale Electro-Structural Characterisation of Ohmic Contacts Formed on P-Type Implanted 4h-SiC. *Nanoscale Res. Lett.* **2011**, *6*.
43. Roccaforte, F.; Giannazzo, F.; Raineri, V. Nanoscale Transport Properties at Silicon Carbide Interfaces. *J. Phys. D-Appl. Phys.* **2010**, *43*, 223001.
44. Sonde, S.; Giannazzo, F.; Raineri, V.; Yakimova, R.; Huntzinger, J. R.; Tiberj, A.; Camassel, J. Electrical Properties of the Graphene/4h-SiC (0001) Interface Probed by Scanning Current Spectroscopy. *Phys. Rev. B* **2009**, *80*, 241406.
45. Giannazzo, F.; Roccaforte, F.; Iucolano, F.; Raineri, V.; Ruffino, F.; Grimaldi, M. G. Nanoscale Current Transport through Schottky Contacts on Wide Bandgap Semiconductors. *J. Vac. Sci. Technol. B* **2009**, *27*, 789–794.
46. Radmacher, M.; Cleveland, J. P.; Fritz, M.; Hansma, H. G.; Hansma, P. K. Mapping Interaction Forces with the Atomic Force Microscope. *Biophys. J.* **1994**, *66*, 2159–2165.
47. Radmacher, M.; Fritz, M.; Cleveland, J. P.; Walters, D. A.; Hansma, P. K. Imaging Adhesion Forces and Elasticity of Lysozyme Adsorbed on Mica with the Atomic Force Microscope. *Langmuir* **1994**, *10*, 3809–3814.
48. James, P. J.; Antognozzi, M.; Tamayo, J.; McMaster, T. J.; Newton, J. M.; Miles, M. J. Interpretation of Contrast in Tapping Mode AFM and Shear Force Microscopy. A Study of Nafion. *Langmuir* **2000**, *17*, 349–360.
49. Rotsch, C.; Radmacher, M. Mapping Local Electrostatic Forces with the Atomic Force Microscope. *Langmuir* **1997**, *13*, 2825–2832.
50. Wang, Z. B.; Helander, M. G.; Greiner, M. T.; Qiu, J.; Lu, Z. H. Analysis of Charge-Injection Characteristics at Electrode-Organic Interfaces: Case Study of Transition-Metal Oxides. *Phys. Rev. B* **2009**, *80*.
51. Wagenpfahl, A.; Rauh, D.; Binder, M.; Deibel, C.; Dyakonov, V. S-Shaped Current-Voltage Characteristics of Organic Solar Devices. *Phys. Rev. B* **2010**, *82*.
52. Gonzalez-Vazquez, J. P.; Morales-Florez, V.; Anta, J. A. How Important Is Working with an Ordered Electrode to Improve the Charge Collection Efficiency in Nanostructured Solar Cells? *J. Phys. Chem. Lett.* **2012**, *3*, 386–393.
53. Street, R. A. Localized State Distribution and Its Effect on Recombination in Organic Solar Cells. *Phys. Rev. B* **2011**, *84*.
54. Wagenpfahl, A.; Deibel, C.; Dyakonov, V. Organic Solar Cell Efficiencies under the Aspect of Reduced Surface Recombination Velocities. *IEEE J. Sel. Top. Quantum Electron.* **2010**, *16*, 1759–1763.
55. Hains, A. W.; Liu, J.; Martinson, A. B. F.; Irwin, M. D.; Marks, T. J. Anode Interfacial Tuning Via Electron-Blocking/Hole-Transport Layers and Indium Tin Oxide Surface Treatment in Bulk-Heterojunction Organic Photovoltaic Cells. *Adv. Funct. Mater.* **2010**, *20*, 595–606.
56. Dongaonkar, S.; Servaites, J. D.; Ford, G. M.; Loser, S.; Moore, J.; Gelfand, R. M.; Mohseni, H.; Hillhouse, H. W.; Agrawal, R.; Ratner, M. A.; Marks, T. J.; Lundstrom, M. S.; Alam, M. A. Universality of Non-Ohmic Shunt Leakage in Thin-Film Solar Cells. *J. Appl. Phys.* **2010**, *108*.
57. Xue, J. G.; Uchida, S.; Rand, B. P.; Forrest, S. R. 4.2% Efficient Organic Photovoltaic Cells with Low Series Resistances. *Appl. Phys. Lett.* **2004**, *84*, 3013–3015.
58. Peumans, P.; Yakimov, A.; Forrest, S. R. Small Molecular Weight Organic Thin-Film Photodetectors and Solar Cells. *J. Appl. Phys.* **2003**, *93*, 3693–3723.
59. Brumbach, M.; Placencia, D.; Armstrong, N. R. Titanyl Phthalocyanine/C-60 Heterojunctions: Band-Edge Offsets and Photovoltaic Device Performance. *J. Phys. Chem. C* **2008**, *112*, 3142–3151.
60. Hotchkiss, P. J.; Li, H.; Paramonov, P. B.; Paniagua, S. A.; Jones, S. C.; Armstrong, N. R.; Bredas, J. L.; Marder, S. R. Modification of the Surface Properties of Indium Tin Oxide with Benzylphosphonic Acids: A Joint Experimental and Theoretical Study. *Adv. Mater.* **2009**, *21*, 4496–+.
61. Paniagua, S. A.; Hotchkiss, P. J.; Jones, S. C.; Marder, S. R.; Mudalige, A.; Marrikar, F. S.; Pemberton, J. E.; Armstrong, N. R. Phosphonic Acid Modification of Indium-Tin Oxide Electrodes: Combined Xps/Ups/Contact Angle Studies. *J. Phys. Chem. C* **2008**, *112*, 7809–7817.
62. Pingree, L. S. C.; MacLeod, B. A.; Ginger, D. S. The Changing Face of Pedot: PSS Films: Substrate, Bias, and Processing

Effects on Vertical Charge Transport. *J. Phys. Chem. C* **2008**, *112*, 7922–7927.
63. Irwin, M. D.; Servaites, J.; Buchholz, D.; Leever, B.; Liu, J.; Emery, J.; Zhang, M.; Song, J.; Durstock, M.; Freeman, A.; Bedzyk, M.; Hersam, M.; Chang, R.; Ratner, M.; Marks, T. Structural and Electrical Functionality of NiO Interfacial Films in Bulk Heterojunction Organic Solar Cells. *Chem. Mater.* **2011**, *23*, 2218–2226.
64. Brumbach, M.; Veneman, P. A.; Marrikar, F. S.; Schulmeyer, T.; Simmonds, A.; Xia, W.; Lee, P.; Armstrong, N. R. Surface Composition and Electrical and Electrochemical Properties of Freshly Deposited and Acid-Etched Indium Tin Oxide Electrodes. *Langmuir* **2007**, *23*, 11089–11099.
65. Hotchkiss, P. J.; Jones, S. C.; Paniagua, S. A.; Sharma, A.; Kippelen, B.; Armstrong, N. R.; Marder, S. R. The Modification of Indium Tin Oxide with Phosphonic Acids: Mechanism of Binding, Tuning of Surface Properties, and Potential for Use in Organic Electronic Applications. *Acc. Chem. Res.* **2012**, *45*, 337–346.
66. Hanson, E. L.; Guo, J.; Koch, N.; Schwartz, J.; Bernasek, S. L. Advanced Surface Modification of Indium Tin Oxide for Improved Charge Injection in Organic Devices. *J. Am. Chem. Soc.* **2005**, *127*, 10058–10062.
67. Bruner, E. L.; Koch, N.; Span, A. R.; Bernasek, S. L.; Kahn, A.; Schwartz, J. Controlling the Work Function of Indium Tin Oxide: Differentiating Dipolar from Local Surface Effects. *J. Am. Chem. Soc.* **2002**, *124*, 3192–3193.
68. Wagner, P.; Hegner, M.; Guentherodt, H.-J.; Semenza, G. Formation and *in Situ* Modification of Monolayers Chemisorbed on Ultraflat Template-Stripped Gold Surfaces. *Langmuir* **1995**, *11*, 3867–3875.
69. Stamou, D.; Gourdon, D.; Liley, M.; Burnham, N. A.; Kulik, A.; Vogel, H.; Duschl, C. Uniformly Flat Gold Surfaces: Imaging the Domain Structure of Organic Monolayers Using Scanning Force Microscopy. *Langmuir* **1997**, *13*, 2425–2428.
70. Tang, C. W. 2-Layer Organic Photovoltaic Cell. *Appl. Phys. Lett.* **1986**, *48*, 183–185.
71. Tang, C. W.; Vanslyke, S. A. Organic Electroluminescent Diodes. *Appl. Phys. Lett.* **1987**, *51*, 913–915.
72. Tang, J. X.; Lau, K. M.; Lee, C. S.; Lee, S. T. Substrate Effects on the Electronic Properties of an Organic/Organic Heterojunction. *Appl. Phys. Lett.* **2006**, *88*.
73. Alloway, D. M.; Graham, A. L.; Yang, X.; Mudalige, A.; Colorado, R.; Wysocki, V. H.; Pemberton, J. E.; Randall Lee, T.; Wysocki, R. J.; Armstrong, N. R. Tuning the Effective Work Function of Gold and Silver Using ω-Functionalized Alkanethiols: Varying Surface Composition through Dilution and Choice of Terminal Groups. *J. Phys. Chem. C* **2009**, *113*, 20328–20334.
74. Gaillard, N. Method to Assess the Grain Crystallographic Orientation with a Submicronic Spatial Resolution Using Kelvin Probe Force Microscope. *Appl. Phys. Lett.* **2006**, *89*, 154101.
75. Peisert, H.; Knupfer, M.; Schwieger, T.; Auerhammer, J. M.; Golden, M. S.; Fink, J. Full Characterization of the Interface between the Organic Semiconductor Copper Phthalocyanine and Gold. *J. Appl. Phys.* **2002**, *91*, 4872–4878.
76. Matsushima, T.; Adachi, C. Observation of Extremely High Current Densities on Order of Ma/Cm(2) in Copper Phthalocyanine Thin-Film Devices with Submicron Active Areas. *Jpn. J. Appl. Phys. 2 - Lett.* **2007**, *46*, L1179–L1181.
77. Yamamoto, H.; Kasajima, H.; Yokoyama, W.; Sasabe, H.; Adachi, C.: Extremely-High-Density Carrier Injection and Transport over 12000 a/Cm(2) into Organic Thin Films. *Appl. Phys. Lett.* **2005**, *86*.
78. Sharma, A.; Haldi, A.; Potscavage, W. J.; Hotchkiss, P. J.; Marder, S. R.; Kippelen, B. Effects of Surface Modification of Indium Tin Oxide Electrodes on the Performance of Molecular Multilayer Organic Photovoltaic Devices. *J. Mater. Chem.* **2009**, *19*, 5298–5302.
79. Street, R. A.; Song, K. W.; Cowan, S. Influence of Series Resistance on the Photocurrent Analysis of Organic Solar Cells. *Org. Electron.* **2011**, *12*, 244–248.
80. Techane, S.; Baer, D. R.; Castner, D. G. Simulation and Modeling of Self-Assembled Monolayers of Carboxylic Acid Thiols on Flat and Nanoparticle Gold Surfaces. *Anal. Chem.* **2011**, *83*, 6704–6712.
81. Mandal, H. S.; Kraatz, H. B. : Effect of the Surface Curvature on the Secondary Structure of Peptides Adsorbed on Nanoparticles. *J. Am. Chem. Soc.* **2007**, *129*, 6356–+.
82. Weeraman, C.; Yatawara, A. K.; Bordenyuk, A. N.; Benderskii, A. V. Effect of Nanoscale Geometry on Molecular Conformation: Vibrational Sum-Frequency Generation of Alkanethiols on Gold Nanoparticles. *J. Am. Chem. Soc.* **2006**, *128*, 14244–14245.
83. Smith, R. K.; Lewis, P. A.; Weiss, P. S. Patterning Self-Assembled Monolayers. *Prog. Surf. Sci.* **2004**, *75*, 1–68.
84. Beebe, J. M.; Kim, B.; Gadzuk, J. W.; Frisbie, C. D.; Kushmerick, J. G. Transition from Direct Tunneling to Field Emission in Metal-Molecule-Metal Junctions. *Phys. Rev. Lett.* **2006**, *97*.
85. Engelkes, V. B.; Beebe, J. M.; Frisbie, C. D. Analysis of the Causes of Variance in Resistance Measurements on Metal-Molecule-Metal Junctions Formed by Conducting-Probe Atomic Force Microscopy. *J. Phys. Chem. B* **2005**, *109*, 16801–16810.
86. Wold, D. J.; Frisbie, C. D. Fabrication and Characterization of Metal−Molecule−Metal Junctions by Conducting Probe Atomic Force Microscopy. *J. Am. Chem. Soc.* **2001**, *123*, 5549–5556.